

# Algorithmic Simplification of Neural Networks with Mosaic-of-Motifs

Pedram Bakhtiarifard, Tong Chen, Jonathan Wenshøj, Erik B Dam,  
Raghavendra Selvan

Department of Computer Science, University of Copenhagen, Denmark  
 {pba,raghav}@di.ku.dk

## Abstract

Large-scale deep learning models are well-suited for compression. Methods like pruning, quantization, and knowledge distillation have been used to achieve massive reductions in the number of model parameters, with marginal performance drops across a variety of architectures and tasks. This raises the central question: *Why are deep neural networks suited for compression?* In this work, we take up the perspective of algorithmic complexity to explain this behavior. We hypothesize that the parameters of trained models have more structure and, hence, exhibit lower algorithmic complexity compared to the weights at (random) initialization. Furthermore, that model compression methods harness this reduced algorithmic complexity to compress models. Although an unconstrained parameterization of model weights,  $\mathbf{w} \in \mathbb{R}^n$ , can represent arbitrary weight assignments, the solutions found during training exhibit repeatability and structure, making them algorithmically simpler than a generic program. To this end, we formalize the Kolmogorov complexity of  $\mathbf{w}$  by  $\mathcal{K}(\mathbf{w})$ . We introduce a constrained parameterization  $\hat{\mathbf{w}}$ , that partitions parameters into blocks of size  $s$ , and restricts each block to be selected from a set of  $k$  reusable motifs, specified by a reuse pattern (or mosaic). The resulting method, *Mosaic-of-Motifs* (MoMos), yields algorithmically simpler model parameterization compared to unconstrained models. Empirical evidence from multiple experiments shows that the algorithmic complexity of neural networks, measured using approximations to Kolmogorov complexity, can be reduced during training. This results in models that perform comparably with unconstrained models while being algorithmically simpler.<sup>1</sup>

## 1 Introduction

Better model performance is regularly achieved through scale. Large models, trained on internet-scale datasets with substantial amount of compute, reliably delivers improved performance (Kaplan et al., 2020; Rosenfeld et al., 2019). We observe this trend across many domains, such as computer-vision (Dosovitskiy et al., 2021), multi-modal learning (Radford et al., 2021), and reinforcement-learning (Vinyals et al., 2019). And although new methodologies and architectures undoubtedly contribute to these advances, increases in performance consistently coincides with an increase in model scale and compute.

At the same time, scaling incurs substantial costs in memory, compute and energy (Patterson et al., 2021; Schwartz et al., 2019), which has motivated extensive work on compression techniques, including pruning (Frankle and Carbin, 2019), quantization (Nagel et al., 2021b), distillation (Hinton et al., 2015) and parameter sharing (Pham et al., 2018). This has demonstrated that modern models are often highly redundant and can be reduced by orders of magnitude with limited, or even no degradation in performance (Han et al., 2016). Moreover, it reinforces that sheer scale is not necessarily the linchpin for advances in model capability.

A common notion used to reason about the scale of models is their complexity, which is often associated with parameter count, layer-wise parametrization, or computational cost (Tan and Le, 2020). Such measures correlate with performance and can relate model error with scale (Hestness et al., 2017), yet they remain agnostic to how parameters are structured or reused across model parameters. In this framing, complexity reflects the size of the parameterization and its associated computational footprint, but not the structure of the learned parameters themselves — although the objective of most compression techniques is exactly that of finding redundancies in structure and repeatability. This raises the central question of *Why are models suited for compression?*

<sup>1</sup>Source code <https://github.com/saintslab/MoMos>.

From algorithmic complexity theory, the complexity of an object is the length of the shortest program that generates it (Solomonoff, 1960; Kolmogorov, 1965; Chaitin, 1977). Programs are trivially descriptions of procedures. We hypothesize that optimization generally increases algorithmic regularity, so trained models admit shorter description than (at) random initialization. In our analysis, the object is not the dataset or the learned function, but the *parameterization* itself — that is, the weight matrix, and more specifically its structure rather than the specific numerical values. This differs from prior approaches, such as weight-sharing (Ullrich et al., 2017) and quantization (Hubara et al., 2016; Han et al., 2016) that primarily constrain parameter values. Figure 1 (left) illustrates a weight matrix of a neural network that is randomly initialized, which from the perspective of algorithmic complexity, only has a near trivial description, requiring a program that simply lists all its bits. On the other hand, the weight matrix illustrated in Figure 1 (right) admits a shorter description, as it uses repeating blocks of patterns resulting in an algorithmically simpler objects; such models are well suited for classical compression techniques makes them superior in terms of storage costs (Lempel and Ziv, 1976; loup Gailly and Adler, 1992; Huffman, 1952; Burrows et al., 1994).

Our goal is to impose such simplicity by constraining on repeatability and reuse in parameter space. By restricting the hypothesis class, we show that algorithmic simplicity can be induced, yielding provably shorter descriptions in the worst case and admits compressible models in practice.

From this perspective, our contributions are:

- We present *Mosaic-of-Motifs (MoMos)*, which is a constrained parameterization of model weights; partitioning parameters into blocks of size  $s$ , it restricts each block to be selected from a set of  $k$  reusable motifs, specified by a reuse pattern  $\mathcal{M}$ , referred to as a *mosaic*.
- We show that our parameterization approach guarantees lower worst-case algorithmic complexity, which can further be improved through choices of  $s$  and  $k$ .
- Using proxies for Kolmogorov complexity, we empirically show that MoMos drives learned weights towards algorithmically regular, more compressible, parameterizations than the unconstrained baselines.

While model compressibility have been studied extensively, it is to the best of our knowledge the first work to provide guarantees on the algorithmic complexity of learned parameters by constraining the model class.

## 2 Related work

It has been demonstrated that trained models contain substantial redundancy in their parameter space and are therefore needlessly complex, when complexity is characterized by parameter count, compute and memory cost (Nagel et al., 2021a; Han et al., 2016; Hinton et al., 2015). Vector quantization (Gray, 1984) approaches exploit this redundancy by constraining the latent space to discrete representations (Van Den Oord et al., 2017) or by quantizing weights into fixed vectors and reusing repeated matrix-multiplications to improve downstream efficiency (Gong et al., 2014; Vali and Bäckström, 2023). Similarly, redundancies are identified in weight-sharing approaches to cluster weights, reducing the number of distinct parameters and compressing networks (Wu et al., 2018; Nowlan and Hinton, 1992; Ullrich et al., 2017).

Entropy measures have been proposed as proxies for model complexity by measuring the distribution of weights and activation functions, relating it to generalization behavior (Xu and Raginsky, 2017; Achille and Soatto, 2018), and also to guide optimization trajectories (Chaudhari et al., 2019). However, when weight arrangements induce similar distributions, thus similar entropy values, these proxies cannot, in general, capture algorithmic regularities.

The Minimum Description (MDL) principle argues the shortest description of data relative to a model class and compressor is the best model (Rissanen, 1978; Grunwald, 2004; Grünwald et al., 2008). A distinction to our work is treating the parameterization of model weights as the object whose description length we control, independent of any particular dataset and compressor.

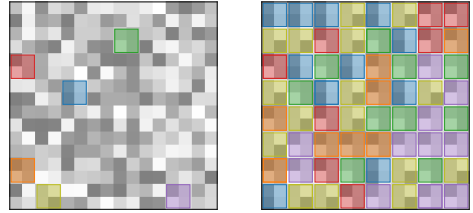


Figure 1: (left) Unconstrained  $16 \times 16$  parameterization with randomly selected motifs highlighted. (right) MoMos parameterization enforcing  $2 \times 2$  motif reuse.

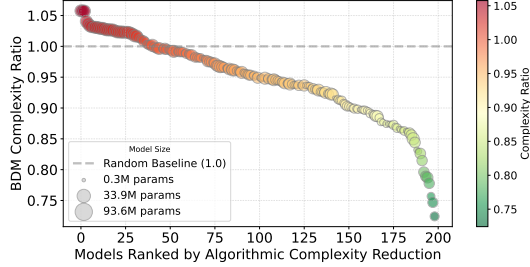


Figure 2: Reduction in algorithmic complexity measured as the ratio of the BDM length of a pretrained model and its corresponding random initialization. The plot shows the BDM complexity ratio (see Section 4) for 110 pretrained models from Pytorch Image Models (TIMM) library with up to 100M trainable parameters.

**Algorithmic Complexity of Binary Objects.** Algorithmic information theory (AIT) defines complexity as the description length of an object itself. The Kolmogorov (Solomonoff, 1960; Kolmogorov, 1965; Chaitin, 1977) complexity of a finite binary string  $\mathbf{w}$ , denoted  $\mathcal{K}(\mathbf{w})$ , is the length of the shortest program  $\mathbf{p}$  that outputs  $\mathbf{w}$  and halts when run on a prefix Turing machine  $U$ . Let  $U$  be a universal prefix Turing machine. For a finite binary string  $\mathbf{x} \in \{0, 1\}^*$ , its Kolmogorov complexity is defined as

$$\mathcal{K}(\mathbf{w}) := \min\{|\mathbf{p}| : U(\mathbf{p}) = \mathbf{w}\}, \quad (1)$$

where  $|\mathbf{p}|$  is the bit-length of the shortest program  $\mathbf{p}$  that outputs  $\mathbf{x}$  and halts.

While  $\mathcal{K}(\cdot)$  is not computable in general, it relates to the algorithmic probability  $\mathcal{P}(\mathbf{w}) = \sum_{\mathbf{p}: U(\mathbf{p})=\mathbf{w}} 2^{-|\mathbf{p}|}$  through the coding theorem  $\mathcal{K}(\mathbf{w}) = -\log \mathcal{P}(\mathbf{w}) + O(1)$ , the probability of randomly generating a program that outputs  $\mathbf{x}$  and halts. For small objects, the Coding Theorem Method (CTM) approximates  $\mathcal{P}(\mathbf{w})$  by the output frequency of  $\mathbf{w}$  on small Turing machines (Soler-Toscano et al., 2014). In practice, the Block Decomposition Method (BDM) scales CTM by summing frequencies of blocks of decomposed objects  $\{\mathbf{b}_i\} \in \mathbf{w}$  (Zenil et al., 2018). The BDM complexity is computed as

$$\mathcal{K}_B(\mathbf{w}) := \sum_i \text{CTM}(\mathbf{b}_i) + \log_2(m_i) \quad (2)$$

where CTM( $\mathbf{b}_i$ ) is the output frequency of the distinct block, and  $m_i$  is the number of occurrences of  $\mathbf{b}_i$  in  $\mathbf{w}$ . Thus frequently occurring blocks increase complexity only by repetition, whereas distinct blocks add description cost.

These techniques have been used to study regularities in learned representations that are not reflected by entropy (Zenil et al., 2018), with recent evidence suggesting that BDM more closely tracks training dynamics in binarized neural networks (Sakabe et al., 2025). Furthermore, analysis of gradient-based training suggest optimization can bias towards lower complexity, shorter description, solutions (Wilson, 2025; Goldblum et al., 2024), which aligns with the idea that reuse reduces description length. Figure 2 provides further evidence that models are compressible because training induces repeatable structure in parameter space, yielding shorter descriptions and lower algorithmic complexity as captured by BDM complexity.

### 3 Mosaic-of-Motifs (MoMos)

Let  $f_{\mathbf{w}}$  denote a model parameterized by weights  $\mathbf{w} = \{\mathbf{w}_\ell\}_{\ell=1}^L$  with  $\mathbf{w}_\ell \in \mathbb{R}^{n_\ell}$  for  $L$  structured components (for example, convolutional kernels or linear layers), where the total number of parameters is  $n = \sum_{\ell=1}^L n_\ell$ . Without loss of generality, we flatten all parameters into a single vector  $\mathbf{w} \in \mathbb{R}^n$ . Let  $q \in \mathbb{N}$  denote the number of bits per weight, then the bit string representing the weights is given as  $\mathbf{w} \in \{0, 1\}^{nq}$ .

For any  $\mathbf{w}$ , there is a trivial description that prints the  $nq$  bits, which implies

$$\mathcal{K}(\mathbf{w}) \leq nq + O(1). \quad (3)$$

The bound in (3) holds for every  $\mathbf{w}$ ; especially for *unstructured* i.e. any description that requires at least  $|\mathbf{w}|$  bits. We aim to induce structure (repeatability of sequences) by defining a restricted hypothesis class where every parameterization then admits a shorter description in the worst case, thereby reducing algorithmic complexity.

We formalize MoMos parameterization for inducing algorithmic simplicity in neural network optimization. Specifically, we define a restricted hypothesis class, where parameter vectors are

guaranteed to admit low algorithmic complexity by constraining their structure and enforcing regularity in the restricted optimization domain. Let  $s \in \mathbb{N}$  denote the block size,<sup>2</sup> and let  $m = \lceil n/s \rceil$  be the number of blocks. Define an invertible slicing operator

$$\psi : \mathbb{R}^n \rightarrow \mathbb{R}^{s \cdot m}, \quad \psi(\mathbf{w}) = (\mathbf{b}_1, \dots, \mathbf{b}_m), \quad (4)$$

where  $\mathbf{b}_i \in \mathbb{R}^s$  are blocks of length  $s$ . The inverse of the slicing operator is  $\psi^{-1}$  such that:

$$\psi^{-1}(\psi(\mathbf{w})) = \mathbf{w}, \quad \forall \mathbf{w} \in \mathbb{R}^n. \quad (5)$$

**Definition 3.1** (Hypothesis Class). Let  $s \in \mathbb{N}$  and  $1 \leq k \leq m$ . A MoMos parameterization consists of fixed blocks  $\mathcal{Z} = (\mathbf{z}_1, \dots, \mathbf{z}_k)$  with  $\mathbf{z}_i \in \mathbb{R}^s$  referred to as *motifs*, and a reuse pattern  $\mathcal{M} \in [k]^m$ , referred to as a *mosaic* where  $[k] = \{1, \dots, k\}$ . A mosaic decides the arrangement of motifs  $\widehat{\mathbf{b}}_i = \mathbf{z}_{\mathcal{M}(i)}$  replacing  $\mathbf{b}_i$  with motifs from  $\mathcal{Z}$  for  $i \in [m]$ . The mosaic of motifs then make up all parameters of a model. Concretely, the MoMos parameterization is

$$\begin{aligned} \widehat{\mathbf{w}} &= \psi^{-1}(\widehat{\mathbf{b}}_1, \dots, \widehat{\mathbf{b}}_m) \\ &= \psi^{-1}(\mathbf{z}_{\mathcal{M}(1)}, \dots, \mathbf{z}_{\mathcal{M}(m)}) \in \mathbb{R}^n. \end{aligned} \quad (6)$$

The hypothesis class induced by the  $(s, k)$ -MoMos parameterization is

$$\mathcal{H}_{s,k} = \{\widehat{\mathbf{w}} : \mathbf{z}_i \in \mathbb{R}^s, \mathcal{M} \in [k]^m\} \subseteq \mathbb{R}^n \quad (7)$$

denoting the set of all parameterizations that can be represented as  $m$  blocks, each selected from a fixed set of  $k$  motifs with their arrangement defined by the mosaic  $\mathcal{M}$ .

*Remark 3.2* (Granularity and repeatability). We are interested in the regime where  $k \ll m$ , since extensive motif reuse imposes regularity and yields parameterizations that are easier to describe algorithmically. Each motif of size  $s$  is considered the unit of reuse which can take on arbitrary values. In practice, however, we enforce  $\mathbf{z}_1 = \mathbf{0}$ , such that repeating  $\mathbf{z}_1$  induces more sparsity.

The MoMos parameterization imposes repeatability by design and reduces the algorithmic complexity of neural network weights. We show this by estimating a uniform, worst-case upper bound on the description length of any parameterization in its hypothesis class, which is better than the trivial description in (3). Figure 1 illustrates MoMos parameterization where dense weights are mapped to a mosaic of motifs that are repeated.

**Proposition 3.3** (MoMos Complexity Bound). *There exists a constant  $\zeta$ , such that*

$$\mathcal{K}(\widehat{\mathbf{w}}) \leq ks + m \lceil \log_2 k \rceil + \zeta, \quad \forall \widehat{\mathbf{w}} \in \mathcal{H}_{s,k}. \quad (8)$$

This is straightforward to prove, as shown in Appendix A.1, where we do this by construction of a program that reconstructs  $\widehat{\mathbf{w}}$  from motifs and a mosaic.

**Corollary 3.4** (Lower Complexity Regime). *Whenever  $ks + m \lceil \log_2 k \rceil < nq$ , we have*

$$\mathcal{K}(\widehat{\mathbf{w}}) < nq + \zeta, \quad \widehat{\mathbf{w}} \in \mathcal{H}_{s,k} \quad (9)$$

*In particular, the description in Proposition 3.3 is strictly shorter than the trivial description of length  $nq$  bits, up to the same additive constant,  $\zeta$ .*

### 3.1 Geometry of the Constrained Optimization Domain

We have seen how the MoMos parameterization enforces regularity using repeated motifs. These constraints do not directly change the parameter space  $\mathbb{R}^n$ , but restricts the subset over which optimisation is performed. We now look the ramifications of this restriction on the geometry of the optimization domain.

Fix a mosaic  $\mathcal{M} \in [k]^m$ , define the slice of  $\mathcal{H}_{s,k}(\mathcal{M}) \subseteq \mathbb{R}^n$  as the set of weights whose block decomposition  $\psi(\widehat{\mathbf{w}}) = (\widehat{\mathbf{b}}_1, \dots, \widehat{\mathbf{b}}_m)$  satisfies

$$\widehat{\mathbf{b}}_i = \widehat{\mathbf{b}}_j \quad \text{whenever} \quad \mathcal{M}(i) = \mathcal{M}(j). \quad (10)$$

That is, blocks with the same label under  $\mathcal{M}$  are equal.

---

<sup>2</sup>We use a deterministic padding rule that maps  $\mathbf{w}$  to  $\mathbb{R}^{s \cdot m}$  by padding  $s \cdot m - n$  trailing zeros.

**Lemma 3.5** (Linear Component). *Fix  $\mathcal{M} \in [k]^m$  and let  $k_{\mathcal{M}} = |\{\mathcal{M}(1), \dots, \mathcal{M}(m)\}|$  be the number of distinct block variables used by  $\mathcal{M}$ . Then  $\mathcal{H}_{s,k} \subseteq \mathbb{R}^n$  is a linear subspace. If  $s \mid n$ , then*

$$\dim(\mathcal{H}_{s,k}(\mathcal{M})) = sk_{\mathcal{M}} \leq sk. \quad (11)$$

*In general,  $\dim(\mathcal{H}_{s,k}(\mathcal{M})) \leq k_{\mathcal{M}} \leq sk$  when  $s \nmid n$ . Proof in Appendix A.2.*

**Proposition 3.6** (Union of Linear Subspaces). *The MoMos hypothesis class decomposes as*

$$\mathcal{H}_{s,k} = \bigcup_{\mathcal{M} \in [k]^m} \mathcal{H}_{s,k}(\mathcal{M}). \quad (12)$$

*Since  $|[k]^m| = k^m$ ,  $\mathcal{H}_{s,k}$  is a union of at most  $k^m$  linear components, each of dimension at most  $sk$ .*

*Proof.* Every  $\widehat{\mathbf{w}} \in \mathcal{H}_{s,k}$  corresponds to some mosaic  $\mathcal{M} \in [k]^m$  and motif values; fixing  $\mathcal{M}$  and varying the motifs gives  $\mathcal{H}_{s,k}(\mathcal{M})$ . Taking the union over all  $\mathcal{M}$  yields the decomposition, since  $|[k]^m| = k^m$  and each  $\mathcal{H}_{s,k}(\mathcal{M})$  has dimension at most  $sk$  by Lemma 3.5.  $\square$

### 3.2 Distinct Linear Components

Distinct mosaics do not necessarily define distinct subspaces, because the symbols  $[k]$  are only labels for shared (repeated) motifs. Although relabeling the symbols changes  $\mathcal{M}$ , it can leave the induced structure unchanged. For instance, take  $m = 4, k = 2, \mathcal{M} = (1, 2, 1, 2)$  and  $\mathcal{M}' = (2, 1, 2, 1)$ . Here the mosaics are different, yet both impose  $\widehat{\mathbf{b}}_1 = \widehat{\mathbf{b}}_3$  and  $\widehat{\mathbf{b}}_2 = \widehat{\mathbf{b}}_4$ , hence  $\mathcal{H}_{s,2}(\mathcal{M}) = \mathcal{H}_{s,2}(\mathcal{M}')$ . To avoid overcounting mosaics that differ only by relabeling  $[k]$ , we consider each mosaic  $\mathcal{M}$  by the shared block positions it induces.

Assume  $s \mid n$  so  $m = n/s$ . A mosaic  $\mathcal{M} \in [k]^m$  assigns to each block position  $i \in [m]$  a motif index  $\mathcal{M}(i) \in [k]$ . For each  $j \in [k]$ , define

$$P_j(\mathcal{M}) := \{i \in [k] : \mathcal{M}(i) = j\}. \quad (13)$$

This is the set of block positions that use index  $j$ . Some indices may be unused, so we only keep non-empty classes:

$$\mathcal{P}(\mathcal{M}) = \{P_j(\mathcal{M}) : P_j(\mathcal{M}) \neq \emptyset\}. \quad (14)$$

Then  $\mathcal{P}(\mathcal{M})$  is a partition of  $[m]$  into  $k_{\mathcal{M}}$  parts, specifying which blocks are constrained to be equal.

**Proposition 3.7** (Distinctness Criterion). *Assume  $s \mid n$ . For any  $\mathcal{M}, \mathcal{M}' \in [k]^m$ ,*

$$\mathcal{H}_{s,k}(\mathcal{M}) = \mathcal{H}_{s,k}(\mathcal{M}') \iff \mathcal{P}(\mathcal{M}) = \mathcal{P}(\mathcal{M}'). \quad (15)$$

*For intuition, note the slice  $\mathcal{H}_{s,k}(\mathcal{M})$  is determined by which equalities  $\widehat{\mathbf{b}}_i = \widehat{\mathbf{b}}_j$  are enforced;  $\mathcal{P}(\mathcal{M})$  encodes the same equalities without labels. Proof in Appendix A.3.*

This notion of distinctness determines the *richness* of the optimization domain. Following the previous example,  $\mathcal{P}(\mathcal{M}) = \mathcal{P}(\mathcal{M}') = \{\{1, 3\}, \{2, 4\}\}$ , so although the number of mosaics is bounded by  $k^m = 2^4 = 16$ , there are less distinct subspaces in the optimization domain. We find the number of distinct subspaces next.

**Definition 3.8** (Number of Distinct Components). *Assume  $s \mid n$ . Let  $m = n/s$ . For mosaic  $\mathcal{M} \in [k]^m$  there are  $k^m$  components, *some* inducing the same subspace. Let  $\alpha(m, k)$  denote the number of distinct subspaces,*

$$\alpha(m, k) := |\{\mathcal{H}_{s,k}(\mathcal{M}) : \mathcal{M} \in [k]^m\}|. \quad (16)$$

Let  $\text{Stir}(m, i)$  denote the Stirling number of the second kind, i.e., the number of ways to partition a set of  $m$  objects into  $i$  non-empty subsets (Moser and Wyman, 1958). Then by Proposition 3.7, distinct subspaces correspond to partitions of  $\{1, \dots, m\}$  into at most  $k$  subsets, hence

$$\alpha(m, k) = \sum_{i=1}^k \text{Stir}(m, i) < k^m. \quad (17)$$

Moreover,  $\alpha(m, k)$  is non-decreasing in both  $m$  and  $k$ , so increasing the number of blocks  $m$ , or allowing more motifs  $k$ , cannot reduce the number of distinct components.

**Richness of the Optimization Domain.** We have characterized how MoMos parameterization changes the optimization domain by enforcing repeated blocks. For fixed  $(s, k)$ , different mosaics  $\mathcal{M} \in [k]^m$  impose different sets of equalities for blocks  $\hat{\mathbf{b}}_i = \hat{\mathbf{b}}_j$  across the  $m$  block positions, thereby inducing distinct linear components  $\mathcal{H}_{s,k}(\mathcal{M})$ . Specifically,  $\alpha(m, k)$  counts how many such components are distinct and how it *enriches* the optimization domain.

To see the effect of  $k$  on the optimization domain, note that increasing  $k$  cannot decrease  $\alpha(m, k)$ , because it permits additional partitions of  $[m]$ . Decreasing  $s$  increases  $m = \lceil n/s \rceil$ , which increases the number of possible linear components available in the optimization landscape.

**Corollary 3.9** (Exponential Growth). *For  $m \geq 2$  and  $k \geq 2$  we have*

$$\alpha(m, k) \geq \text{Stir}(m, 1) + \text{Stir}(m, 2) = 2^{m-1}, \quad (18)$$

*so the number of distinct components grows exponentially in  $m$ .*

To isolate this growth independent of the motif budget, assume  $s \mid n$  and let  $s \cdot k = c'$  be a constant factor. Then  $\alpha(m, k) = \alpha(n/s, c'/s) =: \beta(s)$  is a function of the block size.

**Proposition 3.10** (Monotonicity of  $\beta(s)$ ). *Fix  $n, c'$  and let  $s_1, s_2 \in \mathbb{N}$  with  $s_1 \mid n$  and  $s_2 \mid n$  and  $s_1 \leq s_2$ . Then,*

$$\beta(s_1) \geq \beta(s_2). \quad (19)$$

*That is,  $\beta(s)$  is monotonically decreasing in  $s$ .*

*Proof.* Let  $m_i = n/s_i$  and  $k_i = c'/s_i$  for  $i \in \{1, 2\}$ . Since  $s_1 \leq s_2$ , we have  $m_1 \geq m_2$  and  $k_1 \geq k_2$ . Because  $\alpha(m, k)$  is increasing in both  $m$  and  $k$

$$\alpha(m_1, k_1) \geq \alpha(m_2, k_1) \geq \alpha(m_2, k_2). \quad (20)$$

Substituting  $\beta(s_i) = \alpha(m_i, k_i)$  gives  $\beta(s_1) \geq \beta(s_2)$ .  $\square$

### 3.3 MoMos Algorithm

We have shown that using the MoMos parameterization yields model parameters within a rich optimization domain that is smaller than the unconstrained parameter space. We next present a simple instantiation of these results to obtain MoMos-parameterized model weights during training.

The definition of  $\mathcal{H}_{s,k}$  is agnostic to how motifs are chosen and how blocks are assigned to motifs. Algorithm 1 summarizes how these choices yield a concrete instantiation of the MoMos construction during training. Each iteration takes a standard optimizer step in  $\mathbb{R}^n$ . It then projects the updated weights into  $\mathcal{H}_{s,k}$  by constructing a motif set  $\mathcal{Z}$ , and a reuse pattern  $\mathcal{M}$ , and reconstructing  $\hat{\mathbf{w}}$  as in (7). In our experiments we randomly select  $k$  motifs which always also includes a fixed zero block, i.e.,  $\mathbf{z}_1 = \mathbf{0}$ .

Our theoretical results apply to  $\mathcal{H}_{s,k}$  independent of these choices; analyzing the tighter subset of  $\mathcal{H}_{s,k}$  induced by a particular construction rule, and designing constructions that further reduce description length are natural future directions.

## 4 Experiments

We empirically characterize how parameters to the MoMos hypothesis class impacts the performance and compressibility, with a focus on whether accuracy varies predictably with algorithmic complexity as constraints are tightened.

**Experimental Setup.** We use MoMos across three different neural network architectures: ResNet20 (He et al., 2016), Tiny-ViT (Wu et al., 2022), and a multi-layered perceptron (MLP) with 5 hidden layers and 256 neurons per layer. All models are trained and evaluated on CIFAR-10 (Krizhevsky, 2009) using the standard 40K/10K/10K train/validation/test splits with a batch size of 128. We augment the dataset during training with random horizontal flip and random crop with 4-pixel padding, and use RandAugment (TorchVision, 2016) which applies two randomly sampled augmentations per image. All models were trained from scratch for a maximum of 200 epochs, with early stopping terminating the run after 20 epochs without improving validation loss. We report standard performance metrics averaged over three random seeds.

For the MLP and Tiny-ViT, we use AdamW (Loshchilov and Hutter, 2019) with learning rate  $3 \times 10^{-4}$  and weight decay  $10^{-2}$ , with Tiny-ViT additionally using images resized to  $224 \times 224$ .

---

**Algorithm 1** MoMos Optimization

---

**input** initialization  $\mathbf{w}_0 \in \mathbb{R}^n$ , block size  $s$ , model capacity  $c \in [0, 1)$ , iterations  $n_T$ , data  $\mathcal{D}$ , loss  $\ell$ , optimizer OPT

**output**  $\hat{\mathbf{w}} \in \mathcal{H}_{s,k}$ , Motifs  $\mathcal{Z}$ , Mosaic  $\mathcal{M}$

- 1:  $m \leftarrow \lceil n/s \rceil$ ,  $k \leftarrow \max\{1, \lfloor c \cdot m \rfloor\}$
- 2: **for**  $t = 1, \dots, n_T$  **do**
- 3:    $\mathbf{w}^{(t)} \leftarrow \text{OPTSTEP}(\mathbf{w}_{t-1}; \mathcal{D}, \ell)$
- 4:    $(\mathbf{b}_1^{(t)}, \dots, \mathbf{b}_m^{(t)}) \leftarrow \psi(\mathbf{w}^{(t)})$
- 5:   Uniformly sample indices  $j_1, \dots, j_k$  from  $[m]$
- 6:   **for**  $i = 1, \dots, k$  **do**
- 7:      $\mathbf{z}_i \leftarrow \mathbf{b}_{j_k}$
- 8:   **end for**
- 9:    $\mathcal{Z}^{(t)} \leftarrow (\mathbf{z}_1^{(t)}, \dots, \mathbf{z}_k^{(t)})$
- 10:   **for**  $i = 1, \dots, m$  **do**
- 11:      $\mathcal{M}^{(t)}(i) \leftarrow \arg \min_{j \in \{1, \dots, k\}} \|\mathbf{b}_i^{(t)} - \mathbf{z}_j^{(t)}\|_2^2$
- 12:   **end for**
- 13:    $\hat{\mathbf{w}}^{(t)} \leftarrow \psi^{-1}(\mathbf{z}_{\mathcal{M}^{(t)}(1)}, \dots, \mathbf{z}_{\mathcal{M}^{(t)}(m)})$
- 14:    $\mathbf{w}_t \leftarrow \hat{\mathbf{w}}^{(t)}$
- 15: **end for**

---

For ResNet20, we train with SGD using learning rate 0.1, momentum 0.9, and weight decay  $10^{-4}$ . Besides full precision FP32 training, we include weight-only scalar quantization baselines trained with quantization aware training (QAT) (Jacob et al., 2018) at  $q \in \{16, 8, 4\}$  bits per weight. Although QAT does not explicitly seek to reduce the algorithmic complexity, it does offer compression and forms a useful baseline for comparison. We apply symmetric uniform fake-quantization to weights during the forward pass with a per-tensor scale. Gradients are computed using the straight-through estimator (Bengio et al., 2013) on the round operation.

**Relative Motif Budget.** Recall that the absolute number of motifs is not comparable across network architectures, since the restriction it induces on the hypothesis class depends on  $m = \lceil n/s \rceil$  through the pattern count  $k^m$  (See. Section 3.2). Therefore we use a relative motif budget, or *capacity*,  $c = k/m$  where  $c \in [0, 1)$  and the motif budget is obtained by discretizing to  $k = \max\{1, \lfloor c \cdot m \rfloor\}$ . This reduces capacity by at most  $1/m$ , since  $k = \lfloor c \cdot m \rfloor$  implies  $c - (k/m) < 1/m$ . We report the performance for  $s = \{2, 4\}$  and  $c = \{0.005, 0.01, 0.05, 0.1\}$ .

**Relative Algorithmic Compression (RAC).** We define the relative algorithmic compression (RAC) rate,  $r_{\mathcal{K}}$  as the ratio of the description length for the baseline model (in Eq. (3)) and that for the MoMos construction obtained from the complexity bound (in Eq. 8),

$$r_{\mathcal{K}} = \frac{\mathcal{K}(\mathbf{w})}{\mathcal{K}(\hat{\mathbf{w}})} \approx \frac{nq}{ksq + m \lceil \log_2 k \rceil}. \quad (21)$$

We ignore the constants and hence the last quantity is an approximation. For QAT, we report the RAC rate as  $32/q$  relative to the length of FP32 model.

**BDM Complexity Ratio.** We also compare the algorithmic complexity of the trained neural network weights,  $\mathbf{w}^*$ , using BDM complexity denoted  $\mathcal{K}_B$  relative to the BDM value of randomly initialized weights  $\mathbf{w}_0$ . To do this, we binarize the weights and report the BDM complexity ratio as:

$$r_{\text{BDM}} = \frac{\mathcal{K}_B(\mathbf{w}^*)}{\mathcal{K}_B(\mathbf{w}_0)}. \quad (22)$$

## 5 Results

**Training Reduces Algorithmic Complexity.** Figure 2 shows the BDM complexity ratio  $r_{\text{BDM}}$  for a wide variety of models. We estimated  $r_{\text{BDM}}$  for 200 models, with <100M parameters, randomly sampled from Pytorch Image Models TIMM (Wightman, 2019). The plot shows majority (>90%) of the models exhibit lower algorithmic complexity at convergence than initialization; this trend is consistent across small and large-scale models.

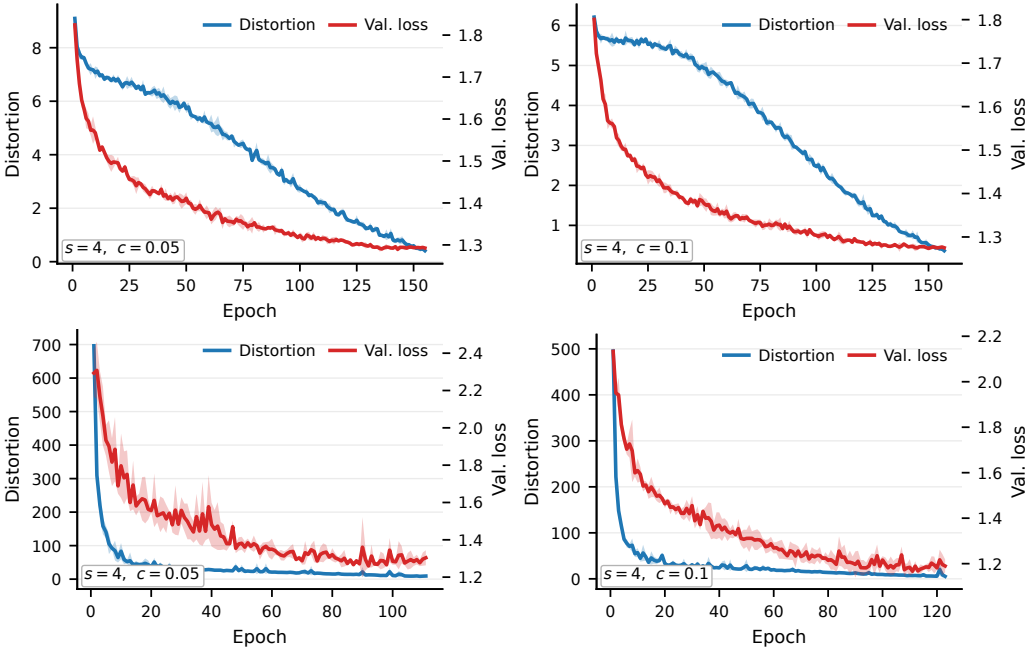


Figure 3: Distortion between the dense weights and the MoMos reconstruction with  $s = 4$  during training of MLP (top row) and Mobile-ViT (bottom row). First and second column is  $c = 0.05, c = 0.1$ , respectively.

**Weight Distortion.** MoMos parameterization of neural network weights introduces approximations to the unconstrained weights as discussed in Section 3.2. Figure 3 shows the difference between the unconstrained weights  $\mathbf{w}$  and MoMos parameterization  $\hat{\mathbf{w}}$ . This is measured as the distortion,  $d = \|\mathbf{w} - \hat{\mathbf{w}}\|^2$ . For both MLP and Mobile-ViT, using  $c = [0.05, 0.1]$ , and  $s = [4]$ , we see the distortion decreases along with the validation loss. This implies that by convergence, the MoMos parameterizations recover the original model. Distortion plots for other models and configurations are shown in Appendix B.1 showing similar behavior.

**Accuracy versus Algorithmic Complexity.** Our main results comparing MoMos parameterization of neural network weights with baseline methods is reported in Table 1. The RAC rate (Eq. (21)) for the baseline model is 1.0, and for the QAT methods it is based on the quantization precision, obtained as  $32/q$ . MoMos parameterizations are reported for several configurations.

The simple MLP used in this work achieves moderate performance for the full precision baseline model. However, it does offer useful insights into how the QAT and MoMos parameterizations compare. Both QAT ( $q = 16, 8$ ) and MoMos ( $s = 2, 4$ ) achieve comparable performance to the baseline model. MoMos generally yields a higher RAC compared to QAT with similar performance. For  $q = 4$  all MoMos with  $s = 4$  and  $c = 0.5, 1$  achieve better performance with also higher RAC.

For ResNet20, MoMos with both  $s = 2, 4$  offer better performance than the QAT baselines. Particularly,  $s = 2, c = 0.1$  yields performance comparable to the baseline performance with a RAC value of  $r_K = 3.1$ . Other configurations offer a variety of trade-offs compared to the QAT models.

With the Tiny-ViT model, these performance gains are accentuated even further. MoMos parameterizations obtain comparable performance with the FP32 model, while yielding up to a RAC rate  $r_K = 9.4$  while using only 0.5% of the total number of block capacity.

We also measure and report the BDM complexity ratio (last column) according to Eq. (2). For all the cases, the BDM complexity decreases inline with our observations for Figure 2. The specific values themselves are not comparable across methods due to the limitations of using the BDM method on binarized model weights.

Similar performance is also observed for Mobile-ViT (Mehta and Rastegari, 2022) which is reported in Table 2 in Appendix B.3.

**Ablation of block size and capacity.** Figure 4 shows the trade-off between validation accuracy and capacity  $c$  for Tiny-ViT as we vary block size  $s$ . For small  $s \in \{2, 4\}$ , the accuracy stays close or above the full precision baseline model with full capacity across the full sweep — even with  $c = 0.01$  capacity. As  $s$  increases, accuracy drops for lower capacities but recovers performance at higher model capacity ( $c > 0.5$ ). This behavior is expected as the optimization space is richer for lower  $s$  as shown in Eq. (3.2). We find consistent trends are found for sweeps with MLP and Resnet20, included in Figure B.2 in Appendix B.2.

Method	Cap.	Config.	MLP			ResNet20			Tiny-ViT		
			Acc.	RAC	$r_{BDM}$	Acc.	RAC	$r_{BDM}$	Acc.	RAC	$r_{BDM}$
Baseline/FP32	100	$q = 32$	$57.80 \pm 0.36$	1.0	0.94	$89.30 \pm 2.64$	1.0	0.75	$81.85 \pm 0.49$	1.0	0.98
QAT	—	$q = 16$	<b><math>57.66 \pm 0.64</math></b>	2.0	0.94	<b><math>81.38 \pm 0.24</math></b>	2.0	0.99	$82.01 \pm 0.49$	2.0	0.98
QAT	—	$q = 8$	$57.63 \pm 0.55$	4.0	0.95	$73.85 \pm 1.05$	4.0	1.00	<b><math>82.51 \pm 0.49</math></b>	4.0	0.98
QAT	—	$q = 4$	$44.35 \pm 1.05$	8.0	0.94	$30.69 \pm 1.19$	8.0	0.87	$48.85 \pm 0.88$	8.0	0.83
MoMos	10	$s = 2$	<b><math>57.68 \pm 0.23</math></b>	3.7	0.94	<b><math>89.77 \pm 3.01</math></b>	3.1	0.75	$81.75 \pm 1.18$	2.5	0.98
MoMos	5	$s = 2$	$57.22 \pm 0.30$	4.5	0.94	$85.47 \pm 1.47$	4.0	0.73	$81.67 \pm 0.66$	3.0	0.99
MoMos	1	$s = 2$	$57.01 \pm 0.13$	6.7	0.93	$84.98 \pm 0.72$	5.5	0.71	<b><math>82.07 \pm 0.35</math></b>	4.1	0.98
MoMos	0.5	$s = 2$	$56.97 \pm 0.27$	7.7	0.90	$81.44 \pm 2.70$	6.2	0.70	$81.43 \pm 0.25$	4.7	0.98
MoMos	10	$s = 4$	<b><math>55.21 \pm 0.42</math></b>	5.3	0.83	<b><math>83.57 \pm 1.39</math></b>	5.0	0.65	$82.59 \pm 0.40$	4.2	0.99
MoMos	5	$s = 4$	$54.93 \pm 0.38$	7.7	0.80	$81.65 \pm 6.60$	7.0	0.61	$82.98 \pm 0.32$	5.5	0.99
MoMos	1	$s = 4$	$53.27 \pm 0.56$	14.3	0.68	$48.74 \pm 24.34$	11.3	0.61	<b><math>83.11 \pm 0.51</math></b>	8.4	0.99
MoMos	0.5	$s = 4$	$52.22 \pm 0.83$	14.3	0.56	$13.08 \pm 5.31$	13.3	0.79	$79.67 \pm 4.06$	9.4	0.99

Table 1: Performance of MLP, ResNet20 and Tiny-ViT on CIFAR10, reported over 3 runs for different motif capacities ( $c$ ), motif size ( $s$ ). Accuracy and the effective algorithmic compression rate ( $r_{\kappa}$ ) are reported. Best performance for the methods between configurations is shown in bold face.

## 6 Discussion

**Parameter Reuse across the Network.** BDM identifies repeating blocks in a bit string to provide a reliable approximation of Kolmogorov complexity ( $\mathcal{K}_B$  in Eq. (2)). We hypothesized that enforcing such block structure within the parameterization of neural networks would yield algorithmically simpler models. Our proposed method, MoMos, achieves this by projecting weight blocks onto random motifs and learning linear subspaces that provide a reasonable approximation of the original, unconstrained optimization space (Section 3). This approach results in weights composed of repeating patterns that are refined during training. As demonstrated by the results in Table 1, MoMos parameterization achieves performance comparable to the full precision model, even at extremely low model capacities (which yield high RAC rates).

**Vector Quantization.** Algorithm 1 shows that the MoMos parameterization shares fundamental similarities with vector quantization (Gray, 1984). Both techniques replace blocks of weights with values from a learned or predefined codebook. However, MoMos employs a global codebook of motifs across the entire neural network, whereas traditional vector quantization methods typically operate per layer or channel to minimize distortion (Gong et al., 2014). Another key distinction lies in the treatment of the codebook itself. In MoMos, the codebook is not learned; instead, we randomly select a set of motifs after each gradient update and project the remaining blocks to their nearest neighbors. Conversely, vector quantization usually involves clustering blocks and assigning centroids to each cluster member; a process that can be computationally expensive if performed at every epoch during training.

**Optimization subspace.** Our analysis in Section 3.2 shows that decreasing the block size  $s$  increases the number of blocks  $m = \lceil n/s \rceil$ , thereby increasing the count of distinct blocks  $\alpha(m, k)$  in  $\mathcal{H}_{s,k}$ . According to Eq. (3.10), for a fixed motif budget, or parameter budget  $k \cdot s$ , a smaller  $s$  creates a richer optimization space by providing the model access to a larger variety of mosaics. This behavior is empirically supported by the results in Figure 4, which show that smaller block sizes yield performance on par with baselines across a broad range of capacities  $c = k/m$ . Conversely, larger  $s$  require significantly higher capacity to recover comparable performance. And although larger  $s$  may enhance the effective algorithmic compression rate, it simultaneously collapses the optimization space and reduces the representational richness for low-capacity regimes. These findings suggest that performance gains at low algorithmic complexity is better achieved by enriching the optimization space than by increasing the number of free parameters, thereby discouraging unnecessary over-parameterization.

### MoMos with Other Compression Methods.

The experiments demonstrate MoMos in full precision mode, with all motifs and indices stored and processed in FP32. However, the benefits of quantizing the motifs  $\mathcal{Z}$  and utilizing lower precision for the mosaic  $\mathcal{M}$  itself can be easily integrated. Such an approach would compound the

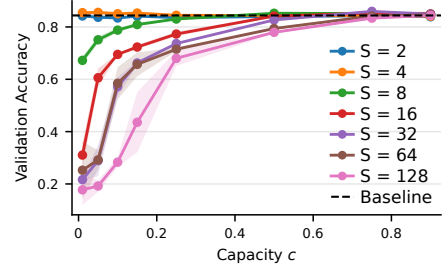


Figure 4: Tiny-ViT MoMos: Validation accuracy over capacity for varying block sizes averaged over three seeds. The dashed line denotes the FP32 baseline.

compression gains of MoMos with the efficiencies of low-precision storage and processing. This compatibility extends to post-training quantization of the MoMos parameterization for further efficiency. Additionally, techniques such as model pruning can be applied at the motif level to achieve even greater gains. Future extensions of this work could naturally include joint pruning and quantization (Wenshøj et al., 2025) within a MoMos-style learning framework.

**Extending Algorithmic Complexity for Deep Learning.** Algorithmic complexity provides a powerful framework for explaining modern deep learning phenomena. To the best of our knowledge, this work represents the first attempt to extend such analyses into a principled method that scales for large-scale deep learning models. While previous studies have utilized these concepts to characterize the training dynamics of small binarized MLPs (Sakabe et al., 2025), we build upon that foundation to present a novel paradigm for model compression. By viewing neural network parameters through the lens of algorithmic simplicity, we shift the focus from traditional redundancy reduction to the process of inducing compressible structures.

**Limitations.** While Kolmogorov complexity proxies such as BDM and RAC serve as useful surrogates in this work, they can occasionally be misleading since they are primarily defined for binary objects. Future research should focus on designing proxies specifically adapted for deep learning, such as BDM variants that employ high-precision quantization and more sophisticated approximations of algorithmic probability instead of the Coding Theorem Method (CTM).

The algorithmic simplification achieved by MoMos does not currently translate into improved hardware utilization. This is not an inherent limitation of the method, but rather a reflection of current hardware acceleration libraries which lack support for fast, reusable block operations. Adapting techniques like fast lookup table (LUT) quantization schemes (Li et al., 2025) could significantly enhance the hardware efficiency of MoMos.

## 7 Conclusion

Over-parameterized deep learning models lend themselves well to compression, which is often attributed to a byproduct of scale. Model compression techniques exploit the redundancies in the neural network parameterization to significantly reduce model size, while retaining most of the performance. In this work, we provide novel insights into the significant redundancies found in neural networks. To this end, we draw upon principles from algorithmic complexity theory, which postulates that truly random objects are incompressible, while non-random models are compressible. Applying this principle, we demonstrate the the algorithmic complexity of randomly initialized neural networks is higher than that of the same model at convergence.

This reduction in complexity suggest an increased occurrence of patterns, or more simply, structure, in the parameterization of neural networks; supporting the claim that learning induces structure and that such structure is compressible. Inspired by BDM, we propose the Mosaic-of-Motifs (MoMos) technique, which constraints the optimization space, such that model parameterizations are more compressible with provably lower worst-case algorithmic complexity. We show that the MoMos parameterized networks are more compressible than those obtained with QAT, with performance comparable to baseline cases. These insights offer a valuable direction for explaining redundancies in deep learning and may foster new directions for future investigation.

**Broader Impact Statement.** This paper presents work whose goal is to advance the field of machine learning. There are many potential societal consequences of our work, none of which we feel must be specifically highlighted here.

**Generative AI Usage Statement** ChatGPT version 5.2 and Google Gemini were used to support programming tasks, including the development of scripts for visualization and setting-up experiments, to edit and refine language and grammar in selected sections of the manuscript.

## Acknowledgments

All authors acknowledge funding from European Union’s Horizon Europe Research and Innovation Action programme under grant agreements No. 101070284, No. 101070408 and No. 101189771. RS also acknowledges funding received under Independent Research Fund Denmark (DFF) under grant agreement number 4307-00143B. Authors thank Eduardo Yuji Sakabe and members of **SAINTS Lab** for valuable discussions.

## References

A. Achille and S. Soatto. Emergence of invariance and disentanglement in deep representations, 2018. URL <https://arxiv.org/abs/1706.01350>.

Y. Bengio, N. Léonard, and A. Courville. Estimating or propagating gradients through stochastic neurons for conditional computation. *arXiv preprint arXiv:1308.3432*, 2013.

M. Burrows, D. J. W. D. I. G. I. T. A. L, R. W. Taylor, D. J. Wheeler, and D. Wheeler. A block-sorting lossless data compression algorithm. 1994. URL <https://api.semanticscholar.org/CorpusID:2167441>.

G. J. Chaitin. Algorithmic information theory. *IBM journal of research and development*, 21(4):350–359, 1977.

P. Chaudhari, A. Choromanska, S. Soatto, Y. LeCun, C. Baldassi, C. Borgs, J. Chayes, L. Sagun, and R. Zecchina. Entropy-sgd: Biasing gradient descent into wide valleys. *Journal of Statistical Mechanics: Theory and Experiment*, 2019(12):124018, 2019.

A. Dosovitskiy, L. Beyer, A. Kolesnikov, D. Weissenborn, X. Zhai, T. Unterthiner, M. Dehghani, M. Minderer, G. Heigold, S. Gelly, J. Uszkoreit, and N. Houlsby. An image is worth 16x16 words: Transformers for image recognition at scale, 2021. URL <https://arxiv.org/abs/2010.11929>.

J. Frankle and M. Carbin. The lottery ticket hypothesis: Finding sparse, trainable neural networks, 2019. URL <https://arxiv.org/abs/1803.03635>.

M. Goldblum, M. A. Finzi, K. Rowan, and A. G. Wilson. Position: The no free lunch theorem, kolmogorov complexity, and the role of inductive biases in machine learning. In R. Salakhutdinov, Z. Kolter, K. Heller, A. Weller, N. Oliver, J. Scarlett, and F. Berkenkamp, editors, *Proceedings of the 41st International Conference on Machine Learning*, volume 235 of *Proceedings of Machine Learning Research*, pages 15788–15808. PMLR, 21–27 Jul 2024. URL <https://proceedings.mlr.press/v235/goldblum24a.html>.

Y. Gong, L. Liu, M. Yang, and L. Bourdev. Compressing deep convolutional networks using vector quantization. *arXiv preprint arXiv:1412.6115*, 2014.

R. Gray. Vector quantization. *IEEE Assp Magazine*, 1(2):4–29, 1984.

P. Grunwald. A tutorial introduction to the minimum description length principle, 2004. URL <https://arxiv.org/abs/math/0406077>.

P. D. Grünwald, P. Vitányi, et al. Algorithmic information theory, 2008.

S. Han, H. Mao, and W. J. Dally. Deep compression: Compressing deep neural networks with pruning, trained quantization and huffman coding, 2016. URL <https://arxiv.org/abs/1510.00149>.

K. He, X. Zhang, S. Ren, and J. Sun. Deep residual learning for image recognition. In *Proceedings of the IEEE Conference on Computer Vision and Pattern Recognition (CVPR)*, pages 770–778. IEEE, 2016.

J. Hestness, S. Narang, N. Ardalani, G. Diamos, H. Jun, H. Kianinejad, M. M. A. Patwary, Y. Yang, and Y. Zhou. Deep learning scaling is predictable, empirically, 2017. URL <https://arxiv.org/abs/1712.00409>.

G. Hinton, O. Vinyals, and J. Dean. Distilling the knowledge in a neural network, 2015. URL <https://arxiv.org/abs/1503.02531>.

I. Hubara, M. Courbariaux, D. Soudry, R. El-Yaniv, and Y. Bengio. Binarized neural networks. *Advances in Neural Information Processing Systems (NeurIPS)*, 2016.

D. A. Huffman. A method for the construction of minimum-redundancy codes. *Proceedings of the IRE*, 40(9):1098–1101, 1952. doi: 10.1109/JRPROC.1952.273898.

B. Jacob, S. Kligys, B. Chen, M. Zhu, M. Tang, A. Howard, H. Adam, and D. Kalenichenko. Quantization and training of neural networks for efficient integer-arithmetic-only inference. In *Proceedings of the IEEE Conference on Computer Vision and Pattern Recognition (CVPR)*, pages 2704–2713. IEEE, 2018.

J. Kaplan, S. McCandlish, T. Henighan, T. B. Brown, B. Chess, R. Child, S. Gray, A. Radford, J. Wu, and D. Amodei. Scaling laws for neural language models, 2020. URL <https://arxiv.org/abs/2001.08361>.

A. N. Kolmogorov. Three approaches to the quantitative definition of information. *Problems of information transmission*, 1(1):1–7, 1965.

A. Krizhevsky. Learning multiple layers of features from tiny images. Technical report, University of Toronto, 2009. URL <https://www.cs.toronto.edu/~kriz/learning-features-2009-TR.pdf>.

A. Lempel and J. Ziv. On the complexity of finite sequences. *IEEE Transactions on Information Theory*, 22(1):75–81, 1976. doi: 10.1109/TIT.1976.1055501.

G. Li, S. Ye, C. Chen, Y. Wang, F. Yang, T. Cao, C. Liu, M. M. S. Aly, and M. Yang. Lut-dla: Lookup table as efficient extreme low-bit deep learning accelerator. In *2025 IEEE International Symposium on High Performance Computer Architecture (HPCA)*, pages 671–684. IEEE, 2025.

I. Loshchilov and F. Hutter. Decoupled weight decay regularization. In *International Conference on Learning Representations (ICLR)*, 2019. URL <https://openreview.net/forum?id=Bkg6RiCqY7>.

J. loup Gailly and M. Adler. gzip: Gnu file compression utility, 1992. URL <https://www.gnu.org/software/gzip/>. Created as a free replacement for Unix compress.

S. Mehta and M. Rastegari. Mobilevit: Light-weight, general-purpose, and mobile-friendly vision transformer, 2022. URL <https://arxiv.org/abs/2110.02178>.

L. Moser and M. Wyman. Stirling numbers of the second kind. *Duke Mathematical Journal*, 1958.

M. Nagel, M. Fournarakis, R. A. Amjad, Y. Bondarenko, M. Van Baalen, and T. Blankevoort. A white paper on neural network quantization. *arXiv preprint arXiv:2106.08295*, 2021a.

M. Nagel, M. Fournarakis, R. A. Amjad, Y. Bondarenko, M. van Baalen, and T. Blankevoort. A white paper on neural network quantization, 2021b. URL <https://arxiv.org/abs/2106.08295>.

S. J. Nowlan and G. E. Hinton. Simplifying neural networks by soft weight-sharing. *Neural Computation*, 4(4):473–493, 07 1992. ISSN 0899-7667. doi: 10.1162/neco.1992.4.4.473. URL <https://doi.org/10.1162/neco.1992.4.4.473>.

D. Patterson, J. Gonzalez, Q. Le, C. Liang, L.-M. Munguia, D. Rothchild, D. So, M. Texier, and J. Dean. Carbon emissions and large neural network training, 2021. URL <https://arxiv.org/abs/2104.10350>.

H. Pham, M. Y. Guan, B. Zoph, Q. V. Le, and J. Dean. Efficient neural architecture search via parameter sharing, 2018. URL <https://arxiv.org/abs/1802.03268>.

A. Radford, J. W. Kim, C. Hallacy, A. Ramesh, G. Goh, S. Agarwal, G. Sastry, A. Askell, P. Mishkin, J. Clark, G. Krueger, and I. Sutskever. Learning transferable visual models from natural language supervision, 2021. URL <https://arxiv.org/abs/2103.00020>.

J. Rissanen. Modeling by shortest data description. *Automatica*, 14(5):465–471, 1978. ISSN 0005-1098. doi: [https://doi.org/10.1016/0005-1098\(78\)90005-5](https://doi.org/10.1016/0005-1098(78)90005-5). URL <https://www.sciencedirect.com/science/article/pii/0005109878900055>.

J. S. Rosenfeld, A. Rosenfeld, Y. Belinkov, and N. Shavit. A constructive prediction of the generalization error across scales, 2019. URL <https://arxiv.org/abs/1909.12673>.

E. Y. Sakabe, F. S. Abrahão, A. Simões, E. Colombini, P. Costa, R. Gudwin, and H. Zenil. Binarized Neural Networks Converge Toward Algorithmic Simplicity: Empirical Support for the Learning-as-Compression Hypothesis. *arXiv preprint arXiv:2505.20646v3*, 2025.

R. Schwartz, J. Dodge, N. A. Smith, and O. Etzioni. Green ai, 2019. URL <https://arxiv.org/abs/1907.10597>.

F. Soler-Toscano, H. Zenil, J.-P. Delahaye, and N. Gauvrit. Calculating kolmogorov complexity from the output frequency distributions of small turing machines. *PLOS ONE*, 9(5):1–18, 05 2014. doi: 10.1371/journal.pone.0096223. URL <https://doi.org/10.1371/journal.pone.0096223>.

R. J. Solomonoff. A preliminary report on a general theory of inductive inference, 1960.

M. Tan and Q. V. Le. Efficientnet: Rethinking model scaling for convolutional neural networks, 2020. URL <https://arxiv.org/abs/1905.11946>.

TorchVision. Torchvision: Pytorch’s computer vision library. <https://github.com/pytorch/vision>, 2016.

K. Ullrich, E. Meeds, and M. Welling. Soft weight-sharing for neural network compression. In *International Conference on Learning Representations*, 2017. URL <https://openreview.net/forum?id=HJGwcKclx>.

M. H. Vali and T. Bäckström. Stochastic optimization of vector quantization methods in application to speech and image processing. In *ICASSP 2023-2023 IEEE International Conference on Acoustics, Speech and Signal Processing (ICASSP)*, pages 1–5. IEEE, 2023.

A. Van Den Oord, O. Vinyals, et al. Neural discrete representation learning. *Advances in neural information processing systems*, 30, 2017.

O. Vinyals, I. Babuschkin, W. M. Czarnecki, M. Mathieu, A. Dudzik, J. Chung, D. H. Choi, R. Powell, T. Ewalds, P. Georgiev, J. Oh, D. Horgan, M. Kroiss, I. Danihelka, A. Huang, L. Sifre, T. Cai, J. P. Agapiou, M. Jaderberg, A. S. Vezhnevets, R. Leblond, T. Pohlen, V. Dalibard, D. Budden, Y. Sulsky, J. Molloy, T. L. Paine, C. Gulcehre, Z. Wang, T. Pfaff, Y. Wu, R. Ring, D. Yogatama, D. Wünsch, K. McKinney, O. Smith, T. Schaul, T. Lillicrap, K. Kavukcuoglu, D. Hassabis, C. Apps, and D. Silver. Grandmaster level in StarCraft II using multi-agent reinforcement learning. *Nature*, 575(7782):350–354, Nov. 2019.

J. Wenshøj, T. Chen, B. Pepin, and R. Selvan. Codeq: End-to-end joint model compression with dead-zone quantizer for high-sparsity and low-precision networks. *arXiv preprint arXiv:2512.12981*, 2025.

R. Wightman. Pytorch image models. <https://github.com/rwightman/pytorch-image-models>, 2019.

A. G. Wilson. Deep learning is not so mysterious or different. *arXiv preprint arXiv:2503.02113*, 2025.

J. Wu, Y. Wang, Z. Wu, Z. Wang, A. Veeraraghavan, and Y. Lin. Deep  $k$ -means: Re-training and parameter sharing with harder cluster assignments for compressing deep convolutions, 2018. URL <https://arxiv.org/abs/1806.09228>.

K. Wu, J. Zhang, H. Peng, M. Liu, B. Xiao, J. Fu, and L. Yuan. Tinyvit: Fast pretraining distillation for small vision transformers. In *European Conference on Computer Vision (ECCV)*, 2022.

A. Xu and M. Raginsky. Information-theoretic analysis of generalization capability of learning algorithms. *Advances in neural information processing systems*, 30, 2017.

H. Zenil, S. Hernández-Orozco, N. A. Kiani, F. Soler-Toscano, A. Rueda-Toicen, and J. Tegnér. A decomposition method for global evaluation of shannon entropy and local estimations of algorithmic complexity. *Entropy*, 20(8):605, 2018.

## A Proofs for MoMos

### A.1 Proof of Proposition 3.3

Let  $f_{\mathbf{w}}$  be a model parameterized by weights  $\mathbf{w} \in \mathbf{R}^n$ . Choose a deterministic procedure for an encoder  $\text{enc}_q$ , fixing weights to  $q$ -bit representations. The encoder is fixed in the main text, but we formally account for the (constant) cost of specifying the encoding. The bit-string representing the weights is given by  $\mathbf{w} \in \{0, 1\}^{nq}$ . Fix a block size  $s \in \mathbb{N}$ , a motif count  $k \in \mathbb{N}$ , and precision  $q \in \mathbb{N}$ . Then define a slicing operator  $\psi$  with inverse  $\psi^{-1}$  satisfying  $\psi^{-1}(\psi(\mathbf{w})) = \mathbf{w}$ , with  $m = \lceil n/s \rceil$  denoting the number of blocks obtained by slicing  $\mathbf{w}$ .

Let  $\widehat{\mathbf{w}} \in \mathcal{H}_{S,K}$ . By Definition (7), there exist motifs  $\mathcal{Z} = (\mathbf{z}_1, \dots, \mathbf{z}_K)$  with  $\mathbf{z}_k \in \mathbb{R}^s$  and a mosaic  $\mathcal{M} \in \{1, \dots, k\}^m$  such that

$$\widehat{\mathbf{w}} = \psi^{-1}(\mathbf{z}_{\mathcal{M}(1)}, \dots, \mathbf{z}_{\mathcal{M}(m)}). \quad (23)$$

Recall that we use  $\mathcal{K}(\widehat{\mathbf{w}})$  to denote the Kolmogorov complexity of the fixed-precision encoding, i.e.,  $\mathcal{K}(\widehat{\mathbf{w}}) = \mathcal{K}(\text{enc}_q(\widehat{\mathbf{w}}))$ . We will upper bound  $\mathcal{K}(\widehat{\mathbf{w}}) = \text{enc}_q(\widehat{\mathbf{w}})$  by explicitly describing a program that prints  $\text{enc}_q(\widehat{\mathbf{w}})$  and halts.

Consider a program  $\mathbf{p}$  that consists of a fixed decoding and reconstruction routine, followed by finite description that encodes the motifs and the mosaic. Since  $s, k, q$ , and  $n$  are fixed for the  $\mathcal{H}_{s,k}$ , the routine can compute  $m = \lceil n/s \rceil$  and parse input of predetermined length in constant time. For each  $\mathbf{z}_k \in \mathbb{R}^s$  the program encodes the motifs with  $\text{enc}_q$  to a binary string of length  $sq$ . Concatenating the  $k$  motif encodings yields a motif description of length  $ksq$  bits. Then each entry in the motif  $\mathcal{M}(i)$  takes values in  $\{1, \dots, k\}$ . The program encodes each value in this set by a fixed length binary representation of length  $\lceil \log_2 k \rceil$  bits. For example, writing  $\mathcal{M}(i) - 1$  in binary with padding. Concatenating the  $m$  encoding yields a pattern description of length  $m \lceil \log_2 k \rceil$  bits.

The program parses the first  $ksq$  description bits as  $k$  consecutive blocks of length  $sq$ , interpreting them as motifs  $\text{enc}_q(\mathbf{z}_1), \dots, \text{enc}_q(\mathbf{z}_K)$ , and then parses the next  $m \lceil \log_2 k \rceil$  bits as  $m$  encodings of length  $\lceil \log_2 k \rceil$ , producing the mosaic indices  $\mathcal{M}(1), \dots, \mathcal{M}(m)$ . It then forms the sequence of encoded blocks

$$\text{enc}_q(\mathbf{z}_{\mathcal{M}(1)}), \text{enc}_q(\mathbf{z}_{\mathcal{M}(2)}), \dots, \text{enc}_q(\mathbf{z}_{\mathcal{M}(m)}), \quad (24)$$

and concatenates them to obtain the padded encoding length  $ms$ . Finally,  $\mathbf{p}$  discards the last  $(ms - n)q$  bits to satisfy  $\psi^{-1}$ . The result is exactly  $\text{enc}_q(\widehat{\mathbf{w}})$ , which the routine prints before halting.

Let  $\zeta$  denote the length in bits of this routine, including any constant overhead required by the reference universal machine to interpret the description format. The constant  $\zeta$  does not depend on  $\widehat{\mathbf{w}}$ , hence the the full program length satisfies

$$|\mathbf{p}| \leq ksq + m \lceil \log_2 k \rceil + \zeta. \quad (25)$$

Since  $\mathbf{p}$  outputs  $\text{enc}_q(\widehat{\mathbf{w}})$  and halts, the definition of Kolmogorov complexity gives

$$\mathcal{K}(\widehat{\mathbf{w}}) = \mathcal{K}(\text{enc}_q(\widehat{\mathbf{w}})) \leq |\mathbf{p}| \leq ksq + m \lceil \log_2 k \rceil + \zeta, \quad (26)$$

which concludes the proof of 3.3.  $\square$

### A.2 Proof of Lemma 3.5

Fix a mosaic  $\mathcal{M} \in [k]^m$ . Recall that  $\mathcal{H}_{s,k} \subseteq \mathbb{R}^n$  consist of all  $\widehat{\mathbf{w}}$  whose block decomposition  $\psi(\widehat{\mathbf{w}}) = (\widehat{\mathbf{b}}_1, \dots, \widehat{\mathbf{b}}_m)$  satisfies  $\widehat{\mathbf{b}}_i = \widehat{\mathbf{b}}_j$  whenever  $\mathcal{M}(i) = \mathcal{M}(j)$ , equivalently  $\widehat{\mathbf{b}}_i = \mathbf{z}_{\mathcal{M}(i)}$  for some choice of motifs  $\mathcal{Z} = (\mathbf{z}_1, \dots, \mathbf{z}_k)$ .

Let  $z = (\mathbf{z}_1, \dots, \mathbf{z}_k) \in \mathbb{R}^{ks}$  denote the concatenation of all motifs. Define  $F_{\mathcal{M}} : \mathbb{R}^{ks} \rightarrow \mathbb{R}^n$  by

$$F_{\mathcal{M}}(z) = \psi^{-1}(\mathbf{z}_{\mathcal{M}(1)}, \dots, \mathbf{z}_{\mathcal{M}(m)}). \quad (27)$$

By construction, as  $z$  ranges over  $\mathbb{R}^{ks}$ , the image  $\text{Im}(F_{\mathcal{M}})$  is exactly the set of vectors obtained by holding  $\mathcal{M}$  fixed and varying motifs, which is  $\mathcal{H}_{s,k}(\mathcal{M})$ .

The operation  $z \rightarrow (\mathbf{z}_1, \dots, \mathbf{z}_k)$  is linear in  $z$  because it only selects and repeats blocks, and  $\psi^{-1}$  is the composition of concatenation with fixed truncations that discards the padded bits; both are linear maps. Hence  $\mathcal{H}_{s,k} = \text{Im}(F_{\mathcal{M}})$  is a linear subspace of  $\mathbb{R}^n$  and

$$\dim(\mathcal{H}_{s,k}(\mathcal{M})) = \text{rank}(F_{\mathcal{M}}) \leq ks. \quad (28)$$

When  $s \mid n$ , let  $J_{\mathcal{M}} = \{\mathcal{M}(i), \dots, \mathcal{M}(m)\}$  and  $k_{\mathcal{M}} = |J_{\mathcal{M}}|$ . Then only motifs with indices in  $J_{\mathcal{M}}$  affect  $F_{\mathcal{M}}(z)$ . Motifs outside  $J_{\mathcal{M}}$  are unused, thus  $\text{rank}(F_{\mathcal{M}}) \leq sk_{\mathcal{M}}$  and  $\psi^{-1}$  merely concatenates. For each index  $j \in J_{\mathcal{M}}$  pick an index  $i(j) \in \{1, \dots, m\}$  such that  $\mathcal{M}(i(j)) = j$ . Then motif  $\widehat{\mathbf{b}}_{i(j)}$  of  $F_{\mathcal{M}}(z)$  equals  $\mathbf{z}_j$ . Therefore, if  $F_{\mathcal{M}}(z) = 0$ , every used motifs  $\mathbf{z}_j$  must equal 0, which shows that the induced map from the  $sk_{\mathcal{M}}$  ranks of the used motifs to  $\mathcal{H}_{s,k}$  is one-to-one. Hence,  $\text{rank}(\mathcal{F}_{\mathcal{M}}) = sk_{\mathcal{M}}$  and

$$\dim(\mathcal{H}_{s,k}(\mathcal{M})) = sk_{\mathcal{M}} \leq sk \quad \text{when } s \mid n. \quad (29)$$

When  $s \nmid n$ , truncation in  $\psi^{-1}$  can reduce rank, so only the upper bound  $\dim(\mathcal{H}_{s,k}(\mathcal{M})) \leq sk_{\mathcal{M}} \leq sk$  is guaranteed.  $\square$

### A.3 Proof of Proposition 3.7

Assume  $s \mid n$  so that  $m = n/s$  and  $\psi^{-1}$  concatenates without truncating. Fix  $\mathcal{M} \in \{1, \dots, k\}^m$ . Then by definition of  $\mathcal{H}_{s,k}(\mathcal{M})$ , the parameterization  $\widehat{\mathbf{w}} \in \mathbb{R}^n$  belong to  $\mathcal{H}_{s,k}(\mathcal{M})$  if and only if its blocks  $\psi(\widehat{\mathbf{w}}) = (\widehat{\mathbf{b}}_1, \dots, \widehat{\mathbf{b}}_m)$  satisfy  $\widehat{\mathbf{b}}_i = \widehat{\mathbf{b}}_j$  whenever  $\mathcal{M}(i) = \mathcal{M}(j)$ . Thus  $\mathcal{H}_{s,k}(\mathcal{M})$  is determined exactly by the partition  $\mathcal{P}(\mathcal{M})$  of  $\{1, \dots, m\}$  into the non-empty parts  $\{i : \mathcal{M}(i) = j\}$ . If  $\mathcal{P}(\mathcal{M}) = \mathcal{P}(\mathcal{M}')$ , then the equalities enforces for blocks are the same for  $\mathcal{M}$  and  $\mathcal{M}'$ , so the constraints coincide when  $\mathcal{H}_{s,k}(\mathcal{M}) = \mathcal{H}_{s,k}(\mathcal{M}')$ . Conversely, if  $\mathcal{P}(\mathcal{M}) \neq \mathcal{P}(\mathcal{M}')$ , then there exists  $i, j \in \{1, \dots, m\}$  such that  $\mathcal{M}(i) = \mathcal{M}(j)$  but  $\mathcal{M}'(i) \neq \mathcal{M}'(j)$ . Choose blocks such that  $\widehat{\mathbf{b}}_i = \widehat{\mathbf{b}}$  and all other blocks pairwise distinct. Concatenating these blocks defines a parameterization  $\widehat{\mathbf{w}}$  that satisfies the block equalities for one mosaic, but violates them for the other. Hence  $\widehat{\mathbf{w}}$  belongs to exactly one of  $\mathcal{H}_{s,k}(\mathcal{M})$  and  $\mathcal{H}_{s,k}(\mathcal{M}')$ , so the two sets differ.  $\square$ .

## B Additional Results

### B.1 Weight Distortion

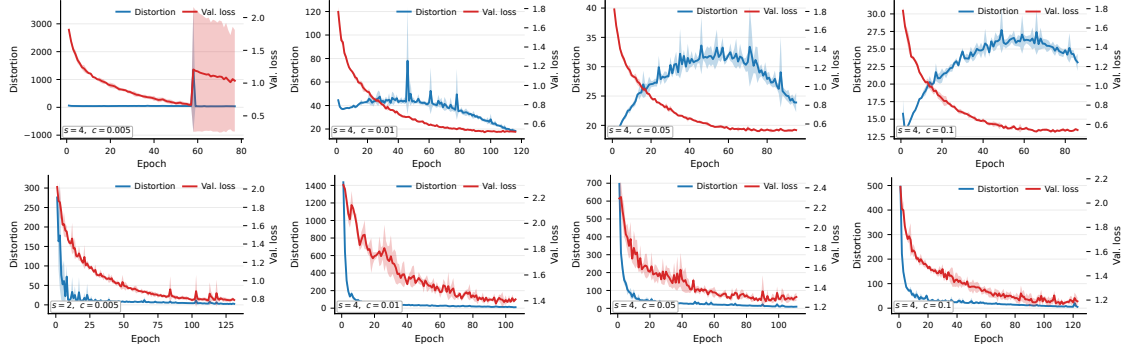


Figure 5: Distortion between the dense weights and the MoMos reconstruction with  $s = 4$  during training of Tiny-ViT (top row) and ResNet20 (bottom row). Columns are arranged as per capacity from left to right:  $c = [0.005, 0.01, 0.05, 0.1]$ .

## B.2 Accuracy Across Block Size and Capacities.

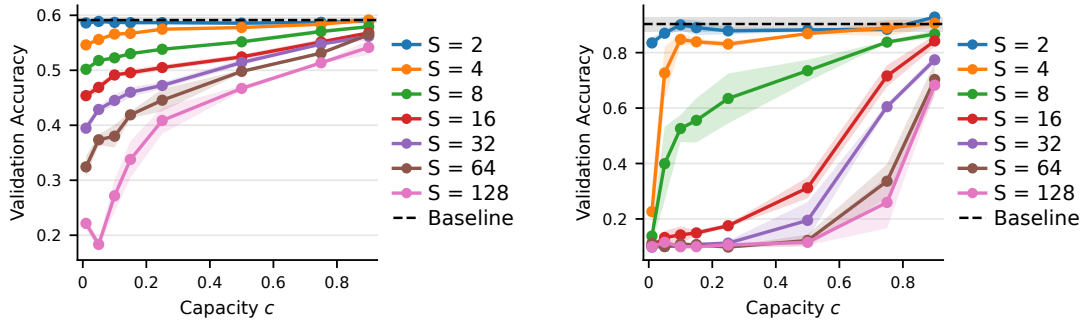


Figure 6: Validation accuracy for (left) MLP and (right) Resnet20 over capacity  $c = \lceil k/m \rceil$  for block sizes  $s$ , averaged over three seeds. The dashed line is the FP32 baseline. Accuracy is close to baseline for small blocks and degrades as  $s$  grows at low  $c$ , while increasing  $c$  recovers baseline performance.

## B.3 Performance for MLP and MobileViT on CIFAR-10

Model	Method	Cap.	Config.	Acc. (%) $\uparrow$	RAC $\uparrow$	$r_{BDM} \downarrow$
	Baseline	100	$q = 32$	$80.27 \pm 0.41$	1	1.01
QAT	–	$q = 16$	<b><math>79.85 \pm 1.17</math></b>	2	1.01	
	–	$q = 8$	$79.15 \pm 0.09$	4	1.01	
	–	$q = 4$	$24.16 \pm 1.19$	8	0.89	
MobileNet	10	$s = 2$	<b><math>77.72 \pm 0.70</math></b>	3.7	1.01	
	5	$s = 2$	$76.82 \pm 0.31$	4.5	1.01	
	1	$s = 2$	$74.84 \pm 0.77$	6.7	1.01	
	0.5	$s = 2$	$72.75 \pm 0.69$	7.7	1.01	
MoMos	10	$s = 4$	<b><math>58.05 \pm 0.56</math></b>	5.3	1.01	
	5	$s = 4$	$55.50 \pm 1.08$	7.7	1.01	
	1	$s = 4$	$50.72 \pm 1.12$	14.3	1.00	
	0.5	$s = 4$	$43.57 \pm 1.60$	14.3	0.99	

Table 2: Performance of MobileViT on CIFAR10, reported over 3 runs for different motif capacities ( $c$ ), motif size ( $s$ ). Accuracy and the effective algorithmic compression rate ( $r_K$ ) are reported. Best performance for the methods between configurations is shown in bold face.